Journal of
Water & Climate Change

IWA PUBLISHING

Journal of Water and Climate Change Vol 15 No 3, 1232 doi: 10.2166/wcc.2024.547

Effect of climate change on soil erosion rate in a tropical Indian catchment

Anbazhagan M.[a,b], Nanditha H. S.[a,b] and Reshmidevi T. V. [a,b,*]

[a] Department of Civil Engineering, B.M.S. College of Engineering, Bengaluru, 560019, India
[b] Visvesvaraya Technological University, Belagavi, Karnataka, India
*Corresponding author. E-mail: reshmidevi.civ@bmsce.ac.in

RT, 0000-0002-3234-3409

ABSTRACT

This study analyzes the variations in soil erosion rate in a tropical catchment in India using the empirical Revised Universal Soil Loss Equation (RUSLE) model integrated with climate change scenarios from an ensemble of global climate models (GCMs) included in the NEX Global Daily Downscaled Projections Coupled Model Intercomparison Project Phase 6 dataset for Shared Socioeconomic Pathways (SSP) 126 and SSP 585. A set of seven GCMs are initially selected. Based on their ability to simulate the rainfall for the current scenario, the PROMETHEE-II method is used to rank the GCMs and the top four best-performing models are used for further analysis. Soil erosion rates projected for the future climate scenarios are compared with the current scenario. In the near future and in the middle of the century, soil erosion rates under the SSP 126 scenario are projected to be higher than that under the SSP 585 scenario. The ensemble average soil erosion rate is projected to increase by 15.41%–25.94% toward the end of the century for different emission scenarios, and the areas susceptible to high and very high soil erosion rates are projected to increase to 40.3%.

Key words: Bhadra catchment, climate change, CMIP-6, revised universal soil loss equation (RUSLE), sediment yield, soil erosion

HIGHLIGHTS

- Climate change impact on the soil loss rate in a tropical catchment is analyzed
- Higher soil loss rates are projected under Shared Socioeconomic Pathways (SSP) 126 scenario in the near future and middle of the century, compared with SSP 585.
- An increase of 15%–25% in the soil loss rate is projected toward the end of the century.
- Areas susceptible to high or very high soil erosion rates are likely to increase from 35.3% to 40.3% toward the end of the century.

1. INTRODUCTION

Approximately, one-third of the global land areas are identified as degraded, with soil erosion considered as the primary factor (Nkonya *et al.* 2016). To implement effective mitigation measures, a scientific understanding of soil erosion across diverse topographic and hydro-climatological conditions is essential. Assessing soil erosion involves evaluating it both locally at a plot or field, and regionally across a landscape, watershed, or over a larger area. Soil erosion evaluation in experimental plots is time-consuming and demands a lot of technological and human resources, which can lead to higher cost of experiments. In addition, there are inhibitions while extrapolating the results to larger watershed or basin scales (Wischmeier & Smith 1978). Modeling simplifies the large-scale soil loss rate determination compared with the *in situ* measurements. Soil erosion models aid in identifying more vulnerable regions within a catchment. For quantifying soil erosion, several empirical models are available, including the Universal Soil Loss Equation (USLE), Modified USLE (MUSLE), and Revised USLE (RUSLE) (Özşahin 2023). Modeling studies for evaluating soil erosion have also been conducted using distributed hydrological models like the Soil and Water Assessment Tool (SWAT) (Mosbahi *et al.* 2013) and the Water Erosion Prediction Project (WEPP) (Landi *et al.* 2011). Among these models, the most commonly used is the RUSLE (Koirala *et al.* 2019; Mohammed *et al.* 2020).

Recent studies from across the world show that soil erosion rates are primarily dependent on rainfall characteristics (Dash & Maity 2023; Weng *et al.* 2023). Global climate change and the associated changes in the precipitation pattern are projected to have a direct impact on soil erosion rates (IPCC 2014; Dash & Maity 2023; Weng *et al.* 2023). Studies on soil erosion rates

under changing climate conditions often utilize precipitation projections from climate models. Most of these studies assume all the other factors including the land use/land cover (LULC) to be constant throughout the future periods (Gupta & Kumar 2017; Doulabian *et al.* 2021). However, a few studies have analyzed the changes in the soil erosion rate in the context of both climate and LULC changes (Maurya *et al.* 2021; Dash & Maity 2023).

When precipitation variations are estimated from global climate models (GCMs) or regional climate models, the soil erosion models inherit the uncertainties from the climate models. To address this issue, recent studies have used multimodel ensembles and different emission scenarios (Reshmidevi *et al.* 2018; Doulabian *et al.* 2021). Several studies are available using the climate models from earlier generations, known as Coupled Model Intercomparison Project (CMIP)-3 (Gupta & Kumar 2017) and CMIP-5 (Maurya *et al.* 2021; Weng *et al.* 2023). The recent-generation CMIP-6 models have been reported to exhibit better statistical consistency over the observed data compared with CMIP-3 and CMIP-5 models (Kim *et al.* 2020; Xin *et al.* 2020). Being a recent addition to the climate model database, changes in the soil erosion rates under the future scenarios projected by these models are yet to be explored for most of areas.

Bhadra River, a tributary of the river Krishna, originates in the Western Ghats in peninsular India. Bhadra dam was constructed across the river, near Bhadravati (Karnataka State) in the year 1965 with a gross storage capacity of 2,025.87 million m^3 and is the major source of irrigation water and hydro-power generation in the area. The current study area encompasses the Bhadra catchment up to the Bhadra reservoir (Figure 1). The catchment receives heavy to very heavy rainfall, with the annual average value greater than 3,000 mm at various places in the upper catchment. The terrain transitions from steep slopes in the Western Ghats to a milder slope towards the catchment outlet. The rainfall also drastically reduces from the upper areas to the lower catchment. Hence, the potential for soil erosion is high in the upper catchment, which gradually reduces toward the lower catchment. This high spatial variation within the catchment can be studied only using regional models focusing on smaller areas.

Soil loss and reservoir sedimentation are concerns in the catchment. A study by the Central Water Commission (CWC) (WS & RS Directorate 2020) has estimated 4.87% loss in the reservoir storage capacity over 47 years to 2011. Previous studies from the area linked this sediment load in the river to the total precipitation and the maximum intensity (KERS 1987; Krishnaswamy *et al.* 2006). Future climate scenarios project increased precipitation and runoff rates in the region (Meenu *et al.* 2013; Pichuka *et al.* 2017). However, these studies are not specifically focused on the Bhadra reservoir and its catchment area and have not considered the impact of projected climate change on soil erosion. This study, therefore, focuses on understanding the possible impacts of climate change on soil erosion in the Bhadra reservoir catchment using empirical soil erosion

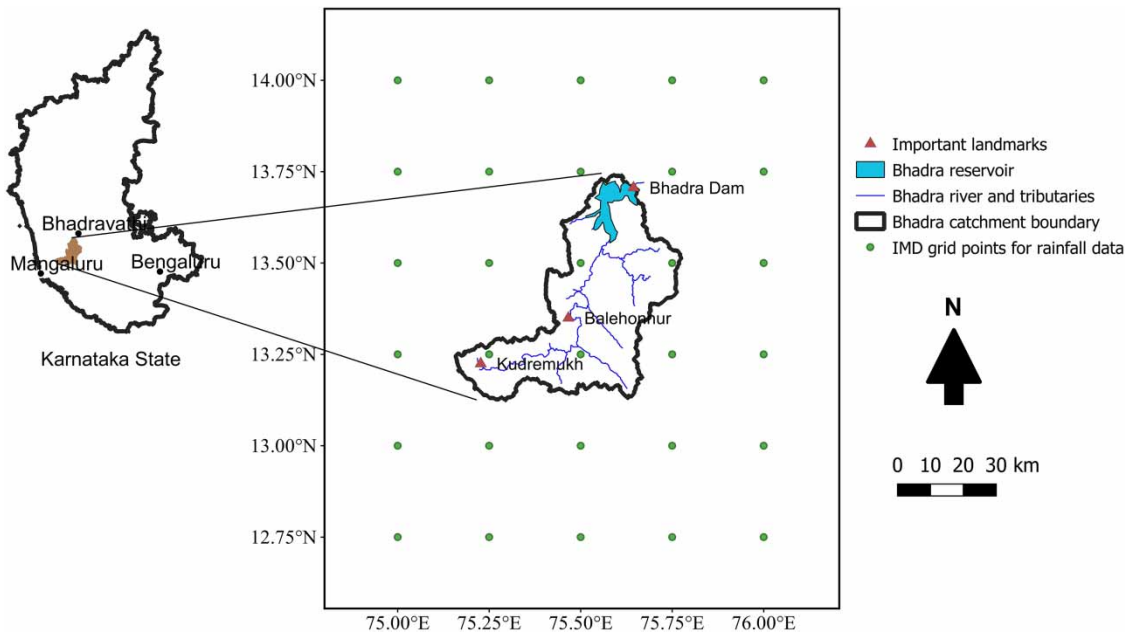

Figure 1 | Location map of the Bhadra catchment.

models and climate projections from CMIP-6 models. Given the extreme hydrological activities combined with the steep topography in the catchment, such studies are essential for the planning and operation of the reservoir located in the river basin.

2. STUDY AREA DATA AND METHODOLOGY

2.1. Study area data

A Shuttle Radar Topographic Mission digital elevation model (DEM) with 30 m spatial resolution (Figure 2(a)) from the United States Geological Survey (USGS) web portal is used to extract the topographical details of the area. A soil map of the area obtained from the FAO is presented in Figure 2(b). The catchment area is dominated by Plinthic Acrisols (Ap) and Eutric Nitosols (Ne) soil types, which are highly erodible under favorable conditions. Daily gridded rainfall data are obtained from the India Meteorological Department (IMD) at a spatial resolution of $0.25° \times 0.25°$ for the 30 grid points (Figure 1) in and around the catchment. Rainfall shows large spatial variation in the area, with average annual rainfall varying from around 3,500 mm in the upper catchment to close to 1,500 mm toward the catchment outlet (Figure 2(c)). Land cover type is depicted through normalized difference vegetation index (NDVI) derived from the satellite images. Using Google Earth Engine, the average NDVI for the period March to May is extracted from the MODIS/MCD43A4_006_NDVI dataset (Figure 2(d)). Higher NDVI values represent forest areas and forest plantation, dominated in the catchment. The negative values near the outlet of the catchment represent the Bhadra reservoir, and the negative values at the upper catchment indicate the Lakya reservoir built to collect the sediment load generated from the Kudremukh mining area. All the maps are prepared at 30 m spatial resolution.

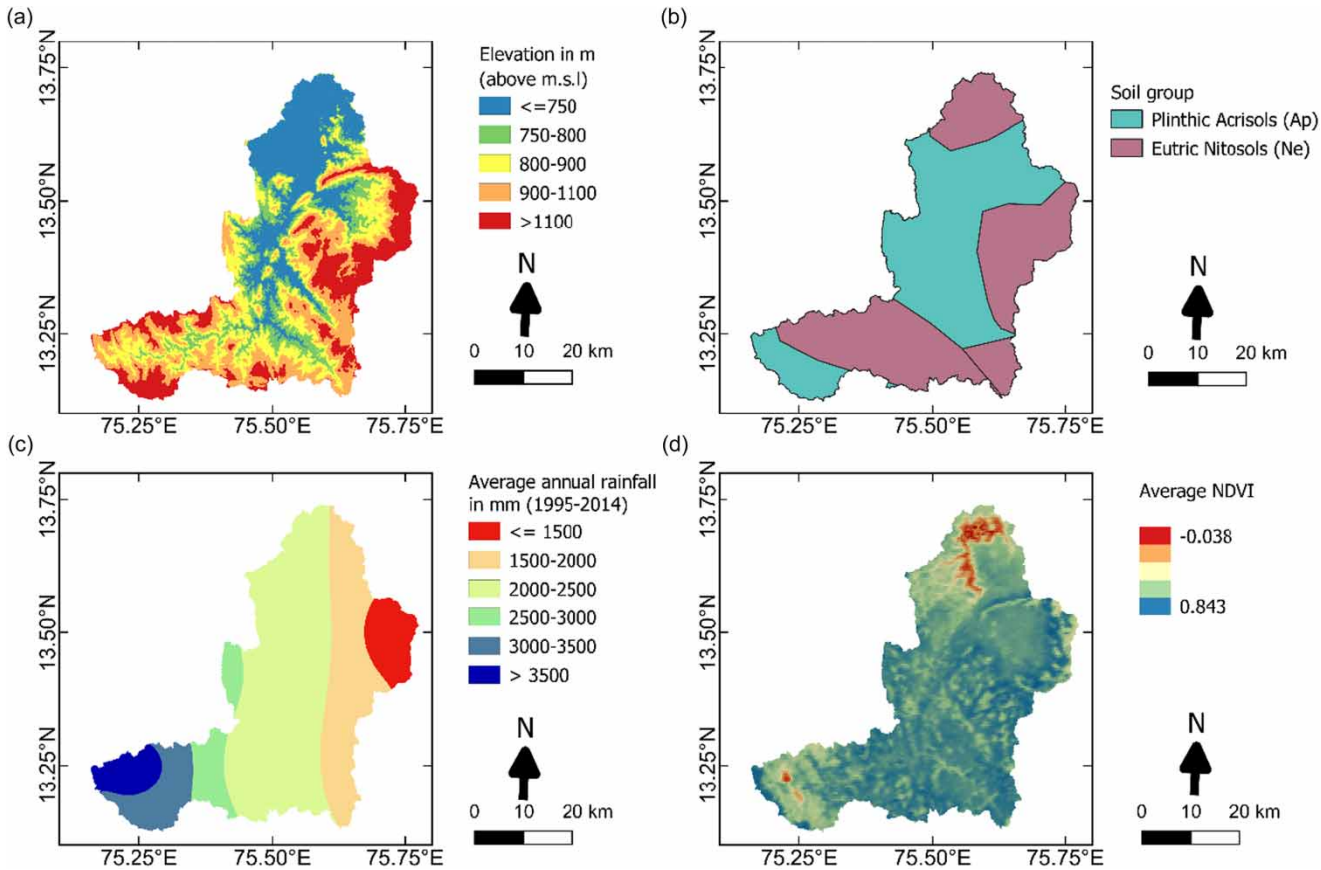

Figure 2 | Various spatial information of the study area required for the modeling: (a) digital elevation model, (b) soil map, (c) annual average rainfall, and (d) average NDVI for March to May.

A recent report by the CWC provides the rate of sedimentation and the loss of reservoir storage capacity, averaged over the period 2007–2011 (WS & RS Directorate 2020). These data are used to establish the relation between the soil erosion rate and the reservoir sedimentation rate in the catchment. This study also uses precipitation projections from the CMIP-6 climate models, as available from the NASA Earth Exchange Global Daily Downscaled Projections dataset (NEX-GDDP CMIP6) for the 0.25° × 0.25° grids (30 points shown in Figure 1) for the current and the future scenarios.

2.2. Methodology

Spatially varying soil erosion rates in the catchment are simulated using the empirical RUSLE model and are used to estimate the sediment yield at the catchment outlet and the reservoir sedimentation. The model is calibrated for the period 2007–2011 using the observed reservoir sedimentation data from the CWC. The calibrated model is later used to study the impact of climate change on the soil erosion rate using precipitation projection from the selected models included in the NASA NEX-GDDP-CMIP-6 dataset. Four time-periods, each of 20 years duration, current scenario (1995–2014), near future (2025–2044), middle of the century (2053–2072), and end of the century (2081–2100), are considered. Two extreme scenarios are incorporated using shared socioeconomic pathway (SSP) 126 with less radiative forcing (2.6 W/m^2 in 2100) and SSP 585 with the highest radiative forcing (8.5 W/m^2 in 2100).

2.2.1. Revised universal soil loss equation

In the RUSLE model, gross soil loss (GSL, t·ha^{-1}·y^{-1}) is determined as a function of rainfall erosivity factor R, soil erodibility factor K, slope length and steepness factor LS, land cover management factor C, and support practice factor P, as shown in Equation (1):

$$\mathrm{GSL} = R.K.\mathrm{LS}.C.P \tag{1}$$

The R factor shows the erosive strength of precipitation. The empirical relation proposed by Nakil & Khire (2016) for Indian catchments is used to calculate R (MJ·mm·ha·h^{-1}·y^{-1}) in terms of the long-term annual rainfall in mm as shown in Equation (2):

$$R = 839.15 \times e^{0.0008\mathrm{AR}} \tag{2}$$

The K factor is a measure of the vulnerability of soil particles to erosion due to rainfall and runoff factors. The relation proposed by Williams *et al.* (1983) is used here to compute the K factor in terms of soil texture. The LS factor, also known as the topographic factor, is calculated considering the slope characteristics using the relation proposed by Wischmeier & Smith (1978). The C factor describes the impact of soil cover, crop management systems, and farming practices on soil erosion. Simple methods to calculate the C factor include the use of a look-up table based on the type of vegetation (Morgan *et al.* 1998) or the relation with the NDVI (van der Knijff *et al.* 2000). For the tropical catchment in this study, the relation between NDVI and the C factor proposed by Durigon *et al.* (2014) and modified by Colman *et al.* (2018) is used. The P factor depicts the impact of the implementation of soil management practices (Renard *et al.* 1997). The value is lower when the management practices are highly effective in reducing soil erosion. If no conservation practices are observed in the catchment, the P factor is assumed to be 1.0. Owing to the difficulty in estimating the P factor from field observations, many studies have ignored it or assumed it to be 1.0 (Adornado *et al.* 2009). In this study, the P factor is set to 0.9, since about 85% of the study area is forest, plantations, and shrubland, with no significant land management practices.

Raster maps of the various RUSLE factors are prepared at 30 m spatial resolution in QGIS (version 3.22.6). The corresponding soil erosion rate is estimated by multiplying these factors as given in Equation (1) at each pixel. The values are spatially averaged to compute the area average soil erosion for the entire catchment.

2.2.2. Future climate scenarios

The capability of the GCMs in simulating the climate scenario varies for different regions, based on the model structure and the parameterization adopted. Moreover, for the same region, intermodel variability is very prominent (Reshmidevi *et al.* 2018; Katzenberger *et al.* 2021). To reduce the uncertainty associated with the use of a single GCM, an ensemble of CMIP-6 GCMs included in the NEX-GDDP dataset is used. Based on the literature (Katzenberger *et al.* 2021; Mitra 2021; Anil & Raj 2022), seven GCMs, namely, BCC-CSM2-MR, EC-EARTH 3, NorESM2-MM, MIROC6, IPSL-CM6A-LR, INM-

CM5-0, and CNRM-CM 6-1, which give reasonably good projection for the Indian region, are chosen. The downscaled data are available at fine spatial resolution (0.25° × 0.25°). To evaluate the reliability of the GCMs in simulating the precipitation scenarios, data are compared with the observed 0.25° × 0.25° gridded rainfall data from the IMD.

Multicriteria decision analysis tool PROMETHEE-II (Brans & Vincke 1985) is used to rank GCMs using three error-based and skill score-based statistical performance indices: SS, correlation coefficient (CC), and root-mean-square error (RMSE). The SS used here indicates the similarity between the probability density functions of the observed data and the GCM-derived precipitation. It is estimated by creating seven bins, following the IMD daily rainfall classification as mentioned in the study by Barde *et al.* (2020) and comparing the frequencies of the observed values and the GCM outputs in each of them (Maxino *et al.* 2008). CC represents the strength of a linear relation between the GCM output and the observed data from the IMD. RMSE is used to represent the average GCM error in precipitation when compared with the IMD data. Weights are assigned to the three indices at each grid point using the entropy method (Raju & Kumar 2014). The entropy E_j (Equation (3)) represents the amount of information available with each of these indices:

$$E_j = -\frac{1}{\ln(N)}\sum_{i=1}^{N} p_{ij}\ln(p_{ij}) \tag{3}$$

where N is the total number of GCMs considered, and p_{ij} is the probability of occurrence of the index j of the ith GCM. A preference function is calculated based on the pairwise comparison between GCMs a and b for the indicator j. Weights derived using the entropy method are used to compute the weighted average preference function known as the multicriterion preference index $\pi(a,b)$ that determines the preference of GCM a over b (Raju & Kumar 2014). The outranking indices $\varphi^+(a)$ and φ^-(a) are then computed using Equations (4) and (5), respectively. Finally, each GCM's net ranking $\varphi(a)$ is computed using Equation (6):

$$\varphi^+(a) = \frac{\sum_N \pi(a,\ b)}{N-1} \tag{4}$$

$$\varphi^-(a) = \frac{\sum_N \pi(b,\ a)}{N-1} \tag{5}$$

$$\varphi(a) = \varphi^+(a) - \varphi^-(a) \tag{6}$$

A higher $\varphi(a)$ value indicates a greater preference for a GCM compared with the others in the group. Using the net ranking $\varphi(a)$, the best-performing GCMs are selected for the study area. Precipitation data from the selected GCMs for the current and future scenarios are used to determine the R factor, and the ensemble average R factor is calculated for the current (1995–2014) and the future periods (near future: 2025–2044, middle of the century: 2053–2072 and end of the century: 2081–2100) for both SSP 126 and SSP 585 scenarios. Using the changing R factor, the corresponding variations in the soil erosion rate under these scenarios are estimated, assuming all the other factors of the RUSLE to be invariant over the periods.

3. RESULTS AND DISCUSSION

3.1. RUSLE model validation

The RUSLE model is calibrated for the Bhadra catchment by using the observed sediment yield data for the period 2007–2011. Annual rainfall time series from the IMD for the same period is used to calculate the R factor at the 30 grid points in and around the catchment. These values are spatially interpolated using an inverse distance weighted interpolation method and the raster map is generated. Spatially averaged R factor for the catchment is calculated as 6,736.21 MJ·mm·ha^{-1}·h^{-1}. The K factor is estimated using the grain size distribution of the soil. The values of characteristics such as percentage sand, silt, clay content, and organic carbon of the topsoil for the Plinthic Acrisols (Ap) are 57, 15.6, 27.1, and 1.09 and for the Eutric Nitosols (Ne) are 68.4, 10.5, 21.2, and 0.6, respectively. The corresponding K factors are estimated as 0.128 and 0.134 t·h·ha^{-1}·MJ^{-1}.mm^{-1}, respectively, for Ap and Ne. The LS factor is calculated from the DEM using the slope characteristics. In the study area, the LS factor is found to vary between 78.54 in steep-slope hilly terrains to 0.07 in the valleys close to the river, with a spatial average of 8.62 for the entire catchment. The average NDVI map of the

study area is used to derive the *C* factor. The *C* factor in the study area ranges from 0.051 to 0.008, leading to a spatially averaged value of 0.082. Higher values are observed near the Kudremukh mining areas and in areas characterized by sparse vegetation. A major part of the catchment is the forested area, which shows relatively lower values of *C* factor. The range of values is in close agreement with the general *C* factor values for forest and scrub areas, reported by Morgan *et al.* (1998).

Raster maps of the contributing factors are used to estimate the spatially varying soil loss rates in the study area using the RUSLE model. A higher soil loss rate is observed in the upper catchment area, characterized by higher rainfall, sparse vegetation, mining activities, and hilly terrain (Figure 3). In the middle catchment, due to the extensive forest cover, the soil erosion rate is observed to be low. The average soil loss for the period 2007–2011 is estimated to be 156.45 $t{\cdot}ha^{-1}{\cdot}y^{-1}$.

Sediment delivery ratio (SDR), the ratio of sediment yield at the catchment outlet to gross soil loss from the catchment, is used to estimate the sediment yield at the catchment outlet. The observed average sedimentation rate in the Bhadra reservoir is 9.728 thousand $m^3{\cdot}km^{-2}{\cdot}y^{-1}$ for the period 2007-2011, with the median sediment density of 1,525 $kg{\cdot}m^{-3}$ (WS & RS Directorate 2020). This corresponds to a sediment yield of 148.352 $t{\cdot}ha^{-1}{\cdot}y^{-1}$. Using these data, the SDR is calculated for the current study area as 0.948. The corresponding SDR relation is derived as a function of catchment area *A* in square kilometres as shown in Equation (7):

$$\mathrm{SDR} = 2.459\, A^{-0.125} \tag{7}$$

3.2. Ranking of GCMs

Bias-corrected precipitation projections from the selected seven CMIP-6 GCMs (BCC-CSM2-MR, EC-EARTH 3, NorESM2-MM, MIROC6, IPSL-CM6A-LR, INM-CM5-0, and CNRM-CM6-1), at 0.25° spatial resolution, are downloaded from the NEX-GDDP dataset. Data at the 30 grid points are compared with the observed rainfall data for the current time-period (1995–2014), and the error and skill score indices (CC, RMSE, and SS) are computed as presented in Table 1. Weights for these indices w_j from the entropy method and the net ranking $\varphi(a)$ of the GCMs from the PROMETHEE-II method are also presented in Table 1.

Among the seven GCMs, only two show a positive net ranking, indicating their preference over the others. A negative net ranking does not indicate a model failure, but less preference for the model compared with the model with a positive ranking. The literature recommends the use of an ensemble of GCMs to overcome model uncertainties while simulating future scenarios (Reshmidevi *et al.* 2018; Doulabian *et al.* 2021). Based on the correlation coefficient and RMSE, the ensemble average of the top four GCMs is found to give a better simulation of precipitation for the study area, when compared with the average of the top two GCMs. Therefore, these four GCMs, namely BCC-CSM2-MR, NorESM2-MM, EC-EARTH 3, and MIROC6, are selected for further analysis.

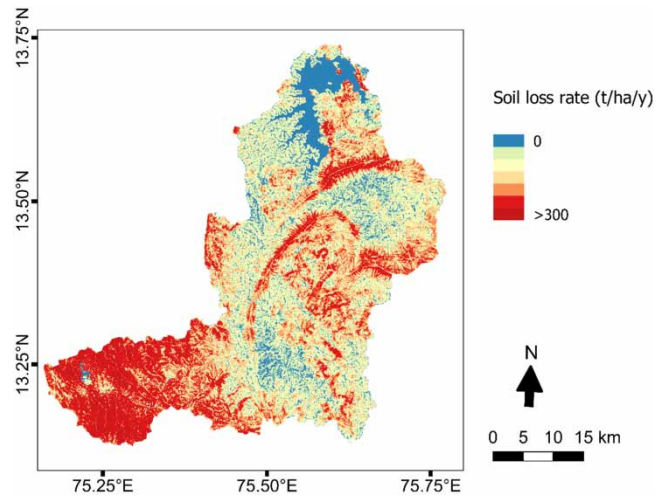

Figure 3 | Spatial variation in the average soil loss rate in the catchment for the period 2007–2011.

Table 1 | GCM performance indices and the ranks derived using PROMETHEE-II method

Indices		CC	RMSE (mm)	SS	$\varphi(a)$	Rank
Weights to the indices w_j		0.52	0.27	0.21	–	–
Models	BCC-CSM2-MR	0.67	193.09	0.78	0.537	1
	NorESM2-MM	0.66	198.36	0.8	0.454	2
	EC-EARTH 3	0.61	209.08	0.82	−0.044	3
	MIROC6	0.62	210.21	0.77	−0.094	4
	IPSL-CM6A-LR	0.61	207.25	0.77	−0.119	5
	INM-CM5-0	0.60	209.59	0.74	−0.345	6
	CNRM-CM6-1	0.59	213.40	0.77	−0.422	7

3.3. Rainfall erosivity factor under the future scenarios

Rainfall simulations from the four selected GCMs are used to estimate the *R* factor for the current (1995–2014) and the three future periods: near future (2025–2044), middle of the century (2053–2072), and end of the century (2081–2100) scenarios, under both SSP 126 and SSP 585, which are compared in Figure 4.

A close analysis of the results shows the intermodel variations in the precipitation simulations and hence in the *R* factor. The variations, though relatively less for the current, near-future, and middle of the century scenarios, are significant for the end of the century scenario. Ensemble average shows an increase in rainfall, and the *R* factor, in the middle of the century followed by a marginal reduction towards the end of the century under SSP 126. Within the SSP 585 scenario, the increase in the *R* factor projected for the middle of the century is expected to increase significantly toward the end of the century.

3.4. Soil erosion rate under the future scenarios

Using the *R* factor for the current and future scenarios, corresponding soil loss rates are estimated, assuming all the other factors such as the soil erodibility factor, topographic factor, cover management factor, and support practice factor to be

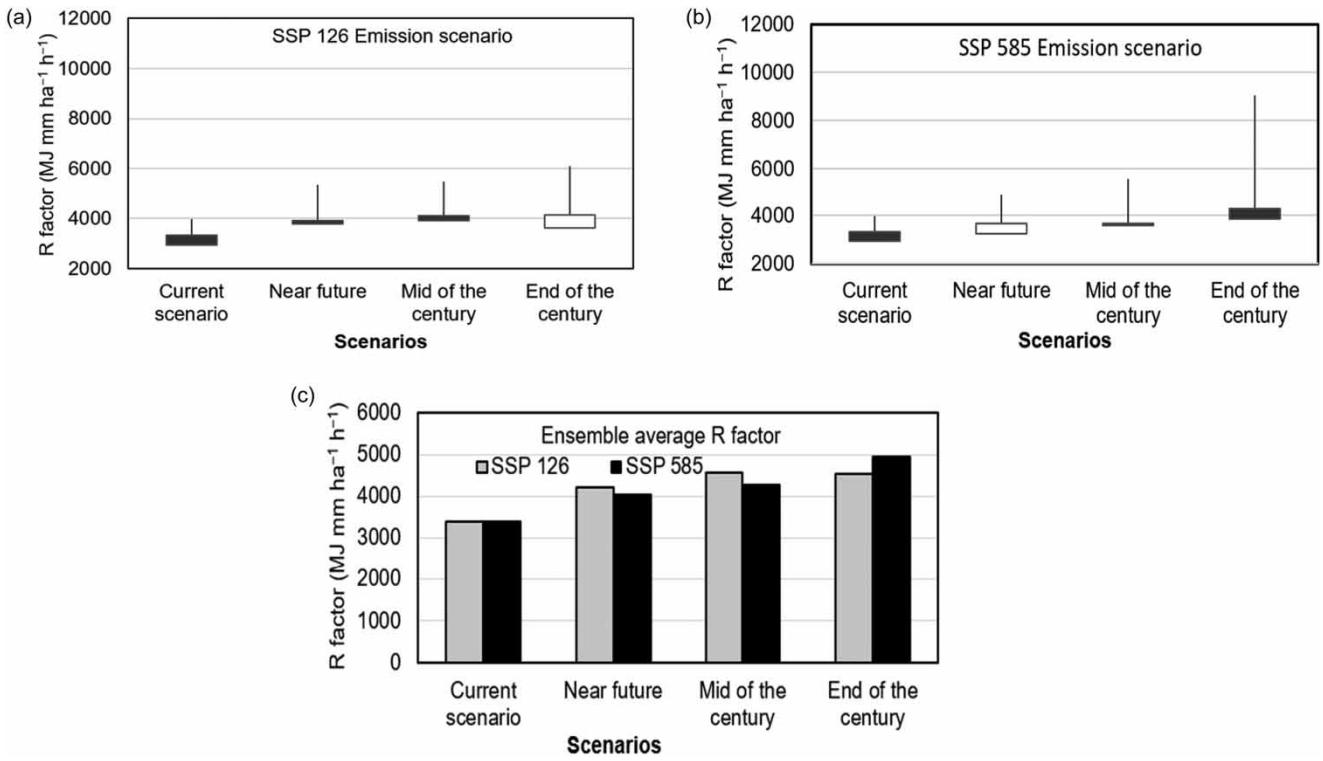

Figure 4 | Comparison of the *R* factor computed from the four GCMs, for different scenarios under (a) SSP 126 and (b) SSP 585 emission scenarios, and (c) the ensemble average.

invariant over all the periods under consideration. The average soil loss rate estimated from the entire catchment area, using the four GCMs and the ensemble average, is given in Table 2. The values obtained under the future scenarios are compared against the baseline scenario (current scenario). The ensemble average soil loss rate under the current scenario is estimated as 54.51 $t \cdot ha^{-1} \cdot y^{-1}$.

The soil loss rate is projected to increase only marginally (3.5%–7.4%) in the near future. However, intensification is projected toward the middle of the century and the end of the century. All the GCMs project an increase in rainfall and hence the soil loss rate in the middle of the century under SSP 126. Toward the end of the century, some of the GCMs show a decline in the soil loss rate, while some others show an increase, with the ensemble average showing a marginal reduction compared with the middle of the century. On the other hand, for the higher emission scenario, all the models, except BCC-CSM2-MR, show an increased soil loss rate in the middle of the century. Further increase toward the end of the century is projected by all the GCMs, except NorESM2-MM.

The presence of modeling uncertainties cannot be ruled out when considering the variations. Therefore, rather than the individual model output, the ensemble average is considered for the detailed analysis. Using the ensemble average, for the near-future scenario, the projected increase in the sediment yield is very minimal. Sediment yield for the middle of the century is projected to increase by 9.46%–15.64% compared with the current scenario. Maximum increase in the sediment yield is projected for the end of the century scenario, which ranges between 15.41% and 25.94%, for different emission scenarios. In the near future and middle of the century, higher soil loss rates under SSP 126 are projected compared with SSP 585. However, projections for SSP 585 show a substantial increase in the soil loss rate from the middle of the century toward the end of the century. Variations in the soil erosion rates are related to the similar variations in the rainfall projected under different future scenarios.

An increase in the soil erosion rate, land degradation, and reservoir sedimentation are some of the major issues in the Krishna basin and its tributaries the Tungabhadra and Bhadra. A study in a segment of the Krishna basin, using the RUSLE model, has reported elevated soil loss rates in regions experiencing higher rainfall, along with significant spatial variations in soil erosion rates in the historical period (Rejani *et al.* 2022). Research conducted in the Tungabhadra basin (Meenu *et al.* 2013) has forecast an increase in precipitation and runoff under the future scenarios, with a more pronounced increase projected under the Special Report on Emissions Scenarios (SRES) A2 scenario compared with the B2 scenario. This is in agreement with the projection for the entire Krishna basin based on an ensemble of CMIP-6 climate models (Anil & Raj 2022), emphasizing large variation in the rainfall projection for different time-periods, SSPs, and spatial locations, with maximum changes projected toward the end of the century under SSP 585. In the near future, for the part of the catchment including the Bhadra basin, more pronounced changes are projected under SSP 126 (−20% to 60%) than under SSP 585 (−20% to 0%). Consistent findings by Kulkarni *et al.* (2014) and Mishra *et al.* (2020) further support increased rainfall projections in the near future under the SSP 126 scenario compared with the SSP 585 scenario for the basins in India. The results are in agreement with the observations of this study, where the maximum changes in the soil erosion rate are projected toward the end of the century under the SSP 585 scenario. In the near-future and middle of century scenarios, more changes

Table 2 | Estimated soil-loss rates under the current and future scenarios

	Soil-loss rate in $t \cdot ha^{-1} \cdot y^{-1}$						
		Near future (2025–2044)		Middle of the century (2053–2072)		End of the century (2081–2100)	
Model	Current scenario (1995–2014)	SSP126	SSP585	SSP126	SSP585	SSP126	SSP585
BCC-CSM2-MR	52.65	55.47	46.85	57.59	51.35	50.98	60.67
NorESM2-MM	56.62	55.23	63.69	74.31	64.19	65.52	58.35
EC-EARTH 3	63.15	72.29	65.82	67.53	74.75	81.69	118.09
MIROC6	49.20	53.29	51.89	55.03	51.99	57.89	54.56
Ensemble average soil-loss rate ($t \cdot ha^{-1} \cdot y^{-1}$)	54.51	58.54	56.41	63.04	59.67	62.91	68.65
Percentage increase in the sediment yield (ensemble average)	–	7.4	3.5	15.64	9.46	15.41	25.94

are projected under SSP 126, compared with the SSP 585 scenario. The projected increase in the soil loss rate is likely to adversely affect the storage capacity of the Bhadra reservoir.

The soil erosion is classified into six classes: negligible (<5 t·ha^{-1}·y^{-1}), very low (5–10 t·ha^{-1}·y^{-1}), low (10–20 t·ha^{-1}·y^{-1}), moderate (20–50 t·ha^{-1}·y^{-1}), high (50–100 t·ha^{-1}·y^{-1}), and very high (>100 t·ha^{-1}·y^{-1}). In all the scenarios, soil erosion rates are negligible or very low in the densely forested area of the catchment and are high or very high in the upper catchment and at higher elevations in the other places. The upper catchment is characterized by heavy rainfall, steep topography, and mining-induced disturbance to the natural environment. Spatial variations of the ensemble average soil erosion under the current scenario and the future scenarios under SSP 585 are shown in Figure 5. Total area with negligible and low soil erosion rates is projected to decline from 20.6% in the current scenario to 18.5% toward the end of the century. As shown in Figure 5, percentage areas susceptible to high or very high soil erosion rates are projected to increase to 40.3% toward the end of the century, compared with 35.3% under the current scenario.

A spatial correlation analysis is performed to identify the sensitivity of the soil loss rate to the RUSLE model factors for the current scenario. The LS factor exhibits a high correlation (0.846), followed by the *R* factor (0.411), while the *K* and *C* factors show a very low correlation (0.02). Assuming constant *P* factor, the soil loss rate is mainly controlled by the topographic factor (LS) and the rainfall erosivity factor (*R*). However, for different time-periods and emission scenarios, the soil factor *K* and the topographic factor LS are considered invariant. To understand the impact of changes in the rainfall pattern on the soil loss rate, crop and soil management factors (*C* and *P* factors) are also assumed constant across the scenarios and

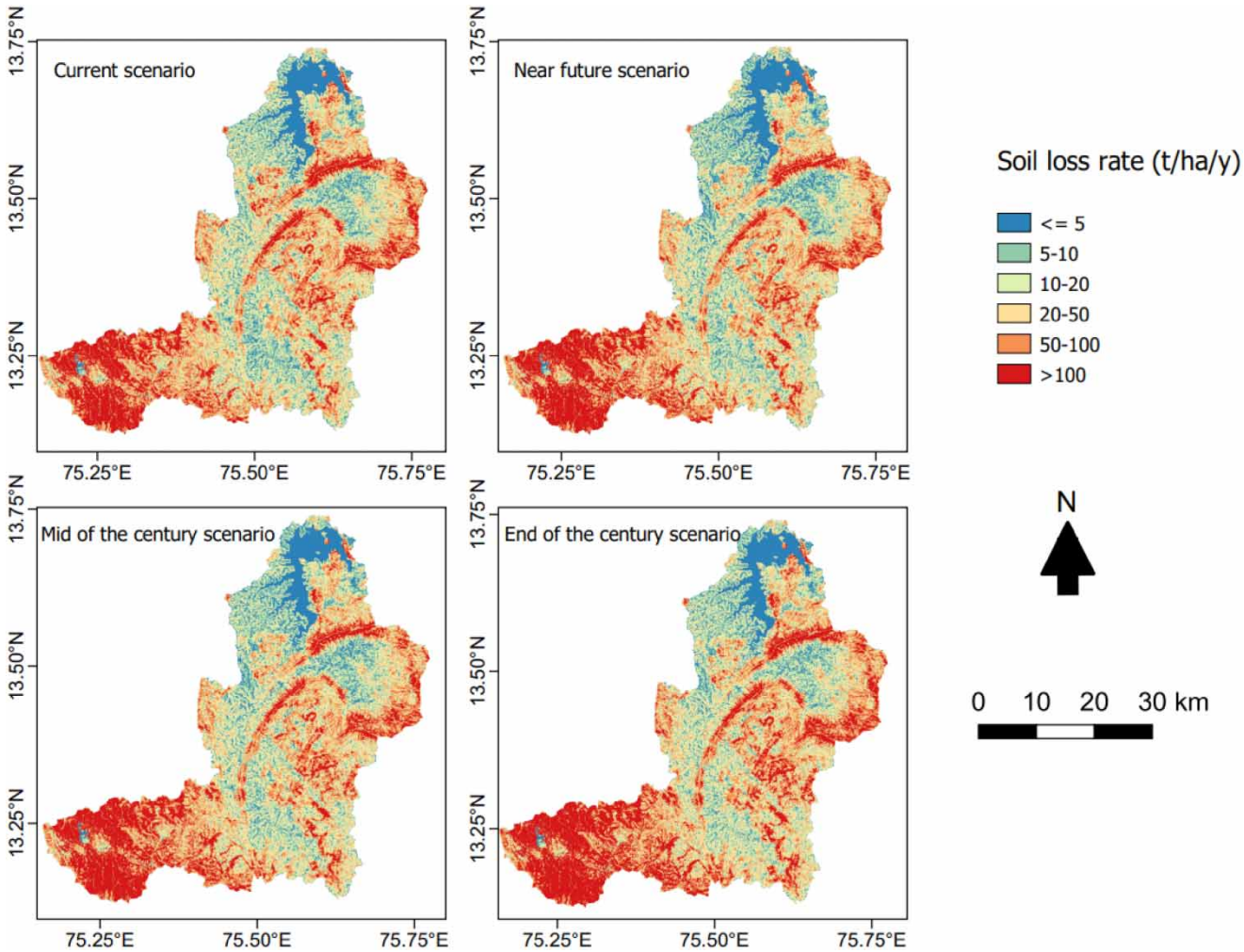

Figure 5 | Ensemble average soil loss rate under the current scenario and SSP 585 future scenarios.

periods considered. The study, therefore, presents the possible impact of rainfall variation under different future scenarios on the gross soil loss rate.

Since the projected increase in the sediment yield is estimated based on the rainfall projections from the GCMs, the values need to be interpreted with caution of uncertainty. The model underestimates sediment yield for the current scenario, suggesting a plausible bias in future estimations as well. Changes in climatic conditions and socioeconomic factors may alter land use/cover types and corresponding RUSLE factors, but in this predominantly forested catchment, such variations are assumed insignificant. More accurate projections need to address the variations in the factors of soil erodibility, topography, cover management, and support practice as well. Though the absolute values of the factors are to be read with caution, all the GCMs consistently project increased soil erosion rate toward the end of the century. This increased soil erosion rate reduces not only the fertility of the catchment but also the storage capacity of the reservoir.

3.5. Mitigation measures

Due to the alarming rate of sedimentation in the reservoirs, the CWC published all the available reservoir sedimentation data (WS & RS Directorate 2020), which serves as a guideline for the procedures and practices to assess the sedimentation and for effective dam rehabilitation in the Indian context. As per this report, the original storage capacity of the Bhadra reservoir was 2,025.87 million m^3, with 1,785.15 million m^3 live storage and 240.72 million m^3 dead storage. Hydrographic surveys conducted in the years 2006 and 2011 estimated a cumulative loss in the storage capacity as 3.01% and 4.87%, respectively, with a significant increase in the sedimentation rate during the period 2006–2011. Over the 47 years till 2011, the storage capacity has been reduced by 95.745 million m^3, impacting the live storage by 75.641 million m^3 (WS & RS Directorate 2020). This affects the crop productivity in the command area. Major crops in the command area are paddy rice followed by sugarcane, areca nut, banana, coconut, and finger millet (Jalikatti & Poddar 2020). Assuming crop water productivity for paddy rice in the Bhadra command area during the rabi season as 0.36 kg/m^3 (Sakthivadivel *et al.* 2019), the dam's reduced live storage is estimated to reduce rabi rice production by around 27,000 tons annually.

The code of practice for control of sediment in reservoirs (IS 6518:1992) recommends appropriate measures to be taken to reduce the inflow of sediments or to arrest their deposition in the reservoir. Table A1 in the Supplementary Material presents a summary of reservoir desilting and sediment management case studies from India. Regular flushing out of the sediments during the flooding season is the most widely adopted approach in India for large dams. However, it is not a viable solution for the Bhadra reservoir. This would transfer sediments downstream, compounding the sedimentation issues in the cascading reservoirs, many of which are already identified as having higher rates of sedimentation. Therefore, desilting through dredging is recommended; nevertheless, economic and environmental challenges cannot be ignored. The reservoir being in the eco-sensitive forest region, proper utilization or disposal planning is required for the safe disposal of the dredged sediments. The *National Framework for Sediment Management* (Ministry of Jal Shakti 2022) recommends a revenue-based model for desilting any reservoir that is used for purposes other than drinking-water supply. Assuming restored storage benefits rabi rice irrigation and hydro-power production, a benefit–cost analysis for the desilting operation is performed as presented in Table 3.

Physical, chemical, and engineering characterization of the dredged sediments is required for estimating its suitability for various applications. Very limited studies are available on the economic value of the dredged reservoir sediments in India. Due to high dredging costs and insufficient data for the economic re-use of the silt, IS 6518:1992 recommends dredging as the last choice, only when all other measures are found ineffective. At the current siltation rate, with present market rates,

Table 3 | Benefit–cost analysis of the Bhadra reservoir dredging

Cost of dredging	Description	Unit cost	Cost of 1 m^3 storage restoration (dredging)
	Hydraulic dredging	Rs. 250/cubic yard	Rs. 329
	Mechanical dredging	Rs. 2,650/cubic yard	Rs. 3,487
Revenue from the restored storage	Description	Unit revenue	Revenue from 1 m^3 storage restored
	Productivity of rabi rice 0.36 kg/m^3	Rs. 2,183/quintal	Rs. 7.86
	Hydropower production 0.05 kWh/m^3	Rs. 6/kWh	Rs. 0.3

the cost of hydraulic dredging is Rs. 2,382.1 million annually. The cost is projected to increase to Rs. 3,004.6 million annually toward the end of the century under SSP 585.

Using the RUSLE model, for the current scenario, the annual loss in the storage capacity is estimated to be 0.34%. This is projected to increase to 0.43% toward the end of the century scenario. CWC guidelines (CWC 2019) categorize this loss rate as medium (0.2%–0.5% per year). Therefore, appropriate treatment of the catchment area to reduce the silt entering the reservoir can be effective in the long-term maintenance of the storage capacity. Implementing gully plugging in the river and contour trenches in the steep slopes can effectively reduce the silt entry to the reservoir. The present study helps to identify the areas of higher soil loss rate, where these measures can be focused on. Very few studies have assessed the effectiveness of these measures in the Bhadra catchment. Regular monitoring of reservoir sedimentation is essential for reservoir operation and maintenance plans. Ground-based and satellite-based remote sensing are powerful tools for regular reservoir monitoring. When satellite-based remote sensing can be used to estimate the water spread area and hence the storage, ground-based remote sensing using LIDAR and echo-sounder can be used for a detailed bathymetric survey of the reservoir and to estimate the sediment deposition (CWC 2019).

4. CONCLUSIONS

The empirical RUSLE model is used to study the impact of climate change on the soil erosion rate in the Bhadra catchment. Climate projections from four GCMs, and two emission scenarios SSP 126 and SSP 585, are used to compute the variation in the rainfall erosivity factor *R*. Corresponding changes in the soil loss rate are projected for the near future (2025–2044), middle of the century (2053–2072), and end of the century (2081–2100) scenarios. The results indicate the spatial variation of the soil erosion rate over the area, predominantly governed by the topography and the rainfall. Soil erosion rate is projected to increase in the future compared with the current scenario (1995–2014). Projected increase in the soil erosion rate is 9.46%–15.64% for the near future and 15.41%–25.94% for the end of the century scenario. Annual loss in the storage capacity is projected to increase from 0.34% under the current scenario to 0.43% toward the end of the century, which is estimated to cause a significant reduction in the rabi rice production in the command area. Approximately 40.3% of the catchment area is likely to experience high to very high soil loss rates towards the end of the century. Appropriate watershed management and soil conservation measures like increasing the vegetation cover, gully plugging, and contour trenches are recommended in the upper catchment to prevent the sediments from reaching the channels. Due to the huge cost of dredging, compared with the benefits, desilting of the reservoir is recommended as the last option. The accuracy of the results depends on the reliability of the GCM projections. Even though the absolute values are subject to variations based on the climate projections, most of the GCMs and the ensemble average show a plausible increase in the soil loss rate under future scenarios, necessitating appropriate actions to check the soil loss rate from the upper catchment area.

ACKNOWLEDGEMENTS

Climate scenarios used were from the NEX-GDDP dataset, prepared by the Climate Analytics Group and NASA Ames Research Center using the NASA Earth Exchange, and distributed by the NASA Center for Climate Simulation (NCCS), which is gratefully acknowledged. The authors also acknowledge USGS for providing SRTM-based digital elevation model used in study; Indian Meteorological Department (IMD) for providing rainfall datasets; and FAO for the soil data used in this study.

DATA AVAILABILITY STATEMENT

All relevant data are available from an online repository or repositories: DEM: https://www.usgs.gov/centers/eros/science/usgs-eros-archive-digital-elevation-shuttle-radar-topography-mission-srtm; soil map: https://www.fao.org/soils-portal/data-hub/soil-maps-and-databases/faounesco-soil-map-of-the-world/en/; NDVI data: https://lpdaac.usgs.gov/tools/data-pool/; rainfall: https://www.imdpune.gov.in/cmpg/Griddata/Rainfall_25_NetCDF.html; GCM precipitation data: https://www.nccs.nasa.gov/services/data-collections/land-based-products/nex-gddp.

CONFLICT OF INTEREST

The authors declare there is no conflict.

REFERENCES

Adornado, H. A., Yoshida, M. & Apolinares, H. A. 2009 Erosion vulnerability assessment in REINA, Quezon Province, Philippines with raster-based tool built within GIS environment. *Agricultural Information Research* **18** (1), 24–31. https://doi.org/10.3173/air.18.24.

Anil, S. & Raj, P. A. 2022 Deciphering the projected changes in CMIP-6 based precipitation simulations over the Krishna River Basin. *Journal of Water and Climate Change* **13** (3), 1389–1407. https://doi.org/10.1287/mnsc.31.6.647.

Barde, V., Nageswararao, M. M., Mohanty, U. C., Panda, R. K. & Ramadas, M. 2020 Characteristics of southwest summer monsoon rainfall events over East India. *Theoretical and Applied Climatology* **141** (3–4), 1511–1528. http://dx.doi.org/10.1007/s00704-020-03251-y.

Brans, J. P. & Vincke, P. 1985 Note – A preference ranking organisation method. *Management Science* **31** (6), 647–656. https://doi.org/10.1287/mnsc.31.6.647.

Colman, C. B., Oliveira, P. T. S., Almagro, A. & Soares-Filho, B. 2018 *Impacts of Climate and Land Use Changes on Soil Erosion in the Upper Paraguay Basin*. Federal University of Mato Grosso do Sul, Campo Grande, MS, Brazil.

CWC 2019 *Handbook for Assessing and Managing Reservoir Sedimentation.* Doc. No. CDSO_GUD_DS_04_v1.0, Central Water Commission, Ministry of Water Resources, River Development & Ganga Rejuvenation, Government of India, New Delhi, India.

Dash, S. S. & Maity, R. 2023 Effect of climate change on soil erosion indicates a dominance of rainfall over LULC changes. *Journal of Hydrology: Regional Studies* **47**, 101373. https://doi.org/10.1016/j.ejrh.2023.101373.

Doulabian, S., Toosi, A. S., Calbimonte, G. H., Tousi, E. G. & Alaghmand, S. 2021 Projected climate change impacts on soil erosion over Iran. *Journal of Hydrology* **598**, 126432.

Durigon, V. L., Carvalho, D. F., Antunes, M. A. H., Oliveira, P. T. S. & Fernandes, M. M. 2014 NDVI time series for monitoring RUSLE cover management factor in a tropical watershed. *International Journal of Remote Sensing* **35** (2), 441–453. https://doi.org/10.1080/01431161.2013.871081.

Gupta, S. & Kumar, S. 2017 Simulating climate change impact on soil erosion using RUSLE model – a case study in a watershed of mid-Himalayan landscape. *Journal of Earth System Science* **126** (3), 43. https://doi.org/10.1007/s12040-017-0823-1.

IPCC 2014 *Climate Change 2014: Impacts, Adaptation, and Vulnerability. Contribution of Working Group II to the Fifth Assessment Report of the Intergovernmental Panel on Climate Change*. IPCC, Geneva, Switzerland.

IS 6518 1992 *Code of Practice for Control of Sediment in Reservoirs*. Bureau of Indian Standards, New Delhi, India.

Jalikatti, V. & Poddar, R. 2020 Productivity of major crops in canal commands of Karnataka state. *International Journal of Agriculture Sciences* **12** (2), 9442–9444.

Katzenberger, A., Schewe, J., Pongratz, J. & Levermann, A. 2021 Robust increase of Indian monsoon rainfall and its variability under future warming in CMIP6 models. *Earth System Dynamics* **12**, 367–386. https://doi.org/10.5194/esd-12-367-2021.

KERS 1987 *Report on Sedimentation Surveys of Bhadra Reservoir*. Karnataka Engineering Research Station, Krishnarajasagara, Karnataka, India.

Kim, Y.-H., Min, S.-K., Zhang, X., Sillmann, J. & Sandstad, M. 2020 Evaluation of the CMIP6 multi-model ensemble for climate extreme indices. *Weather and Climate Extremes* **29**, 100269. https://doi.org/10.1016/j.wace.2020.100269.

Koirala, P., Thakuri, S., Joshi, S. & Chauhan, R. 2019 Estimation of soil erosion in Nepal using a RUSLE modeling and geospatial tool. *Geosciences* **9** (4), 147. https://doi.org/10.3390/geosciences9040147.

Krishnaswamy, J., Bunyan, M., Mehta, V. K., Jain, N. & Karanth, K. U. 2006 Impact of iron ore mining on suspended sediment response in a tropical catchment in Kudremukh, Western Ghats, India. *Forest Ecology and Management* **224** (1–2), 187–198. https://doi.org/10.1016/j.foreco.2005.12.018.

Kulkarni, B. D., Deshpande, N. R., Patwardhan, S. K. & Bansod, S. D. 2014 Assessing hydrological response to changing climate in the Krishna basin of India. *Journal of Earth Science & Climatic Change* **5** (7), 211. https://doi.org/10.4172/2157-7617.1000211.

Landi, A., Barzegar, A. R., Sayadi, J. & Khademalrasoul, A. 2011 Assessment of soil loss using WEPP model and Geographical Information System. *Journal of Spatial Hydrology* **11** (1), 40–51.

Maurya, S., Srivastava, P. K., Yaduvanshi, A., Anand, A., Petropoulos, G. P., Zhuo, L. & Mall, R. K. 2021 Soil erosion in future scenario using CMIP5 models and earth observation datasets. *Journal of Hydrology* **594**, 125851.

Maxino, C. C., McAvaney, B. J., Pitman, A. J. & Perkins, S. E. 2008 Ranking the AR4 climate models over the Murray-Darling Basin using simulated maximum temperature, minimum temperature and precipitation. *International Journal of Climatology* **28**, 1097–1112. https://doi.org/10.1002/joc.1612.

Meenu, R., Rehana, S. & Mujumdar, P. P. 2013 Assessment of hydrologic impacts of climate change in Tunga–Bhadra river basin, India with HEC-HMS and SDSM. *Hydrological Processes* **27**, 1572–1589. https://doi.org/10.1002/hyp.9220.

Ministry of Jal Shakti 2022 *National Framework for Sediment Management*. Department of Water Resources, River Development & Ganga Rejuvenation, Government of India, New Delhi, India.

Mishra, V., Bhatia, U. & Tiwari, A. D. 2020 Bias-corrected climate projections for South Asia from Coupled Model Intercomparison Project-6 (CMIP6). *Scientific Data* **7**, 338. https://doi.org/10.1038/s41597-020-00681-1.

Mitra, A. 2021 A comparative study on the skill of CMIP6 models to preserve daily spatial patterns of monsoon rainfall over India. *Frontiers in Climate* **3**, 654763. https://doi.org/10.3389/fclim.2021.654763.

Mohammed, S., Alsafadi, K., Talukdar, S., Kiwan, S., Hennawi, S., Alshihabi, O., Sharaf, M. & Harsanyie, E. 2020 Estimation of soil erosion risk in southern part of Syria by using RUSLE integrating geo informatics approach. *Remote Sensing Applications: Society and Environment* **20**, 100375. https://doi.org/10.1016/j.rsase.2020.100375.

Morgan, R. P. C., Quinton, J. N., Smith, R. E., Govers, G., Poesen, J. W. A., Auerswald, K., Chisci, G., Torri, D. & Styczen, M. E. 1998 The European Soil Erosion Model (EUROSEM): a dynamic approach for predicting sediment transport from fields and small catchments. *Earth Surface Processes and Landforms* **23**, 527–544. https://doi.org/10.1002/(SICI)1096-9837(199806)23:6%3C527::AID-ESP868%3E3.0.CO;2-5.

Mosbahi, M., Benabdallah, S. & Boussema, M. R. 2013 Assessment of soil erosion risk using SWAT model. *Arabian Journal of Geosciences* **6**, 4011–4019. https://doi.org/10.1007/s12517-012-0658-7.

Nakil, M. & Khire, M. 2016 Effect of slope steepness parameter computations on soil loss estimation: review of methods using GIS. *Geocarto International* **31** (10), 1078–1093. https://doi.org/10.1080/10106049.2015.1120349.

Nkonya, E., Mirzabaev, A. & von Braun, J. 2016 *Economics of Land Degradation and Improvement – A Global Assessment for Sustainable Development*. Springer, Cham, Switzerland

Özşahin, E. 2023 Climate change effect on soil erosion using different erosion models: a case study in the Naip Dam basin, Türkiye. *Computers and Electronics in Agriculture* **207**, 107711. https://doi.org/10.1016/j.compag.2023.107711.

Pichuka, S., Prasad, R. R., Maity, R. & Kunstmann, H. 2017 Development of a method to identify change in the pattern of extreme streamflow events in future climate: application on the Bhadra reservoir inflow in India. *Journal of Hydrology: Regional Studies* **9**, 236–246. https://doi.org/10.1016/j.ejrh.2016.12.084.

Raju, K. S. & Kumar, D. N. 2014 Ranking of global climate models for India using multicriterion analysis. *Climate Research* **60**, 103–117. https://doi.org/10.3354/cr01222.

Rejani, R., Rao, K. V., Shirahatti, M. S., Reddy, K. S., Chary, G. R., Gopinath, K. A., Osman, M., Prabhakar, M. & Singh, V. K. 2022 Spatial estimation of soil loss and planning of suitable soil and water conservation interventions for environmental sustainability in Northern Karnataka in India using geospatial techniques. *Water* **14** (22), 3623. doi:10.3390/w14223623.

Renard, K. G., Foster, G. R., Weesies, G. A., McCool, D. K. & Yoder, D. C. 1997 *Predicting Soil Erosion by Water: A Guide to Conservation Planning with the Revised Universal Soil Loss Equation (RUSLE)*. Agriculture Handbook 703, USDA, Washington, DC, USA.

Reshmidevi, T. V., Kumar, D. N., Mehrotra, R. & Sharma, A. 2018 Estimation of the climate change impact on a catchment water balance using an ensemble of GCMs. *Journal of Hydrology* **556**, 1192–1204. https://doi.org/10.1016/j.jhydrol.2017.02.016.

Sakthivadivel, R., Thiruvengadachari, S. & Amarasinghe, U. A. 2019 *Modernization Using the Structured System Design of the Bhadra Reservoir Project, India: An Intervention Analysis*. Research Report 33, International Water Management Institute, Colombo, Sri Lanka.

van der Knijff, J. M., Jones, R. J. A. & Montanarella, L. 2000 *Soil Erosion Risk Assessment in Europe*. EUR 19044 EN, European Commission Directorate General JRC, Joint Research Centre, Space Applications Institute, European Soil Bureau. https://www.unisdr.org/files/1581_ereurnew2.pdf (accessed on 7 September 2023).

Weng, X., Zhang, B., Zhu, J., Wang, D. & Qiu, J. 2023 Assessing land use and climate change impacts on soil erosion caused by water in China. *Sustainability* **15**, 7865. https://doi.org/10.3390/su15107865.

Williams, J. R., Renard, K. G. & Dyke, P. T. 1983 EPIC: a new method for assessing erosion's effect on soil productivity. *Journal of Soil and Water Conservation* **38** (5), 381–383.

Wischmeier, W. H. & Smith, D. D. 1978 *Predicting Rainfall Erosion Losses: A Guide to Conservation Planning.* Agriculture Handbook 537, USDA, Washington, DC, USA.

WS & RS Directorate 2020 *Compendium on Sedimentation of Reservoirs in India.* Watershed & Reservoir Sedimentation Directorate, Environment Management Organisation, Central Water Commission, New Delhi, India.

Xin, X., Wu, T., Zhang, J., Yao, J. & Fang, Y. 2020 Comparison of CMIP6 and CMIP5 simulations of precipitation in China and the East Asian summer monsoon. *International Journal of Climatology* **40**, 6423–6440. https://doi.org/10.1002/joc.6590.

First received 8 September 2023; accepted in revised form 4 February 2024. Available online 16 February 2024